

Aryl-substituted acridine donor derivatives modulate the transition dipole moment orientation and exciton harvesting properties of donor–acceptor TADF emitters

Ettore Crovini, Kleitos Stavrou, Prakhar Sahay, Bình Minh Nguyễn, Thomas Comerford, Stuart Warriner, Wolfgang Brütting, Andrew Monkman, Eli Zysman-Colman

Angaben zur Veröffentlichung / Publication details:

Crovini, Ettore, Kleitos Stavrou, Prakhar Sahay, Bình Minh Nguyễn, Thomas Comerford, Stuart Warriner, Wolfgang Brütting, Andrew Monkman, and Eli Zysman-Colman. 2024. "Aryl-substituted acridine donor derivatives modulate the transition dipole moment orientation and exciton harvesting properties of donor–acceptor TADF emitters." *The Journal of Physical Chemistry C* 128 (34): 14429–41.
<https://doi.org/10.1021/acs.jpcc.4c03344>.

Aryl-Substituted Acridine Donor Derivatives Modulate the Transition Dipole Moment Orientation and Exciton Harvesting Properties of Donor–Acceptor TADF Emitters

Published as part of *The Journal of Physical Chemistry C* virtual special issue “TADF-Active Systems: Mechanism, Applications, and Future Directions”.

Ettore Crovini, Kleitos Stavrou,* Prakhar Sahay, Binh Minh Nguyễn, Thomas Comerford, Stuart Warriner, Wolfgang Brütting,* Andrew Monkman,* and Eli Zysman-Colman*



Cite This: *J. Phys. Chem. C* 2024, 128, 14429–14441



Read Online

ACCESS |



Metrics & More



Article Recommendations



Supporting Information

ABSTRACT: Thermally activated delayed fluorescence (TADF) compounds are highly attractive as sensitizing and emitting materials for organic light-emitting diodes (OLEDs). The efficiency of the OLED depends on multiple parameters, most of which rely on the properties of the emitter including those that govern the internal quantum and outcoupling efficiencies. Herein, we investigate a series of aryl substituted acridine donor derivatives of the donor–acceptor TADF emitter DMAC-TRZ, with the objective of correlating their properties, such as triplet harvesting efficiency and transition dipole moment orientation, with their corresponding device efficiency. The decoration of the DMAC donor with substituted aryl groups not only modifies the molecular weight and length of the emitter but also affects the emission color and the capacity for the emitters to efficiently harvest triplet excitons. The presence of electron-withdrawing 4-cyanophenyl and 4-trifluoromethylphenyl groups in, respectively, CNPh-DMAC-TRZ and CF₃Ph-DMAC-TRZ, blue-shifts the emission spectrum but slows down the reverse intersystem crossing rate constant (k_{RISC}), while the opposite occurs in the presence of electron-donating groups in ^tBuPh-DMAC-TRZ and OMePh-DMAC-TRZ (red-shifted emission spectrum and faster k_{RISC}). In contrast to our expectations, the OLED performance of the five DMAC-TRZ derivatives does not scale with their degree of horizontal emitter orientation but follows the k_{RISC} rates. This, in turn, demonstrates that triplet harvesting (and not horizontal emitter orientation) is the dominant effect for device efficiency using this family of emitters. Nonetheless, highly efficient OLEDs were fabricated with ^tBuPh-DMAC-TRZ and OMePh-DMAC-TRZ as emitters, with improved EQE_{max} (~28%) compared to the reference DMAC-TRZ devices.



INTRODUCTION

Organic light-emitting diodes (OLEDs) are steadily becoming the dominant display technology across a range of consumer electronic markets, such as smart watches, mobile phones, and televisions. This is thanks to their excellent power efficiency, that they are light in weight, they can produce both saturated colors necessary for ultrahigh definition displays as well as true black, and they can be fabricated on a panoply of substrates, including those that are flexible and transparent.^{1,2} OLEDs are based on a multilayer structure of organic semiconductors sandwiched between two electrodes, where the light-emission results from the electroluminescence of the emitter. The application of current to the device injects electrons and generates holes, which migrate through the device via a so-called hopping mechanism. When these recombine, then an exciton is formed, and it is the radiative decay of the exciton that is responsible for the light that ultimately emanates from

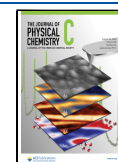
the OLED. Based on the statistics of spin multiplicity, 25% of the exciton formed by their recombination will have singlet multiplicity, and 75% will have triplet multiplicity. In fluorescent compounds, the singlet exciton can decay radiatively, while the triplet exciton cannot due to the spin-forbidden nature of the $T_1 \rightarrow S_0$ transition. Both phosphorescent and thermally activated delayed fluorescent (TADF) materials, however, can harvest both singlet and triplet excitons to produce light, but do so via distinct

Received: May 21, 2024

Revised: July 8, 2024

Accepted: July 8, 2024

Published: August 20, 2024



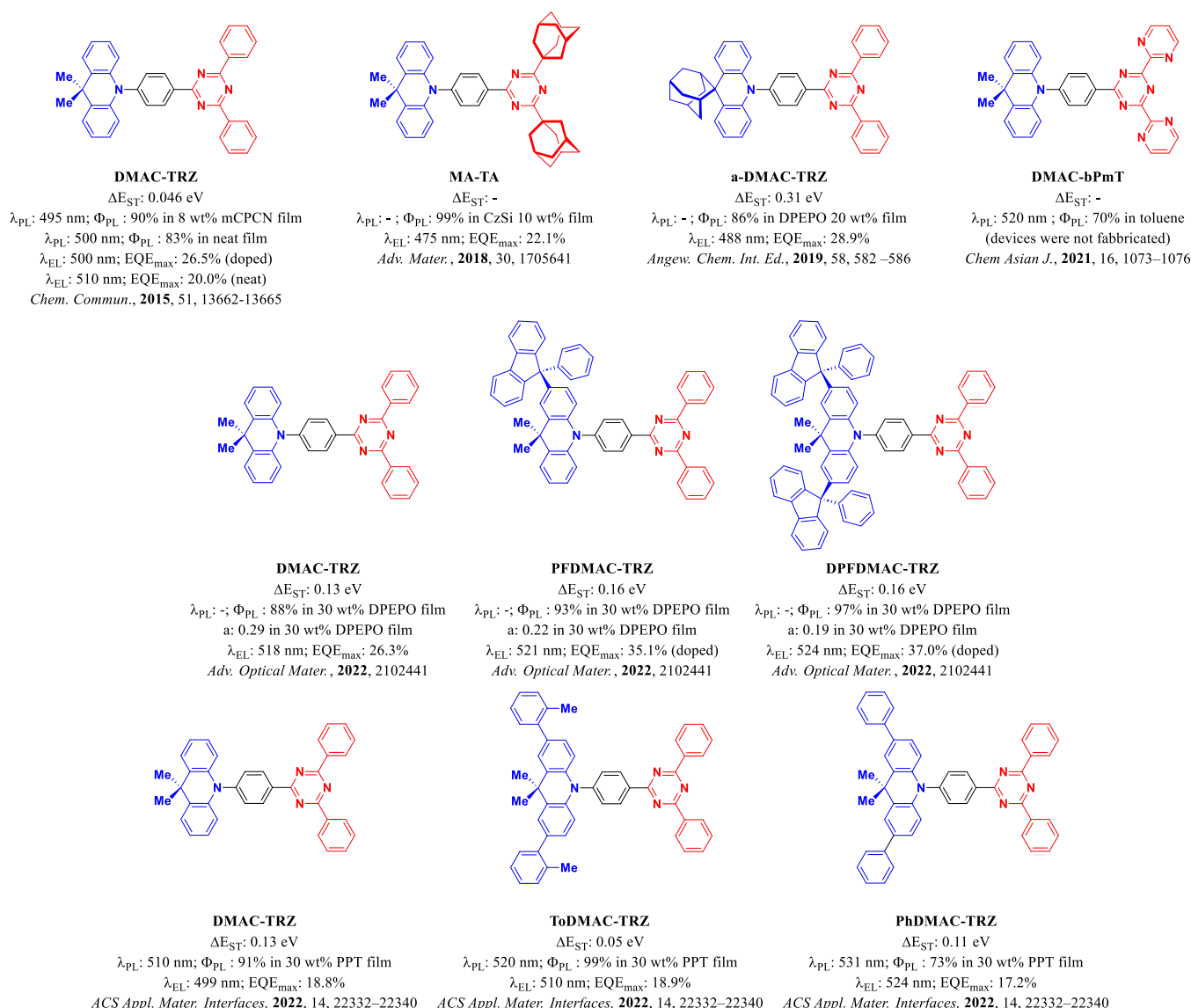


Figure 1. Chemical structure and properties of DMAC-TRZ and several reported derivatives. The variation in reported ΔE_{ST} values of the doped films of DMAC-TRZ originates from a combination of the different doping concentrations, host, and measurement parameters used in each study.

photophysical mechanisms. TADF materials have suitably small energy gaps between the S_1 and T_1 excited states (ΔE_{ST}) that enable triplet excitons to endothermically upconvert to singlets at ambient temperatures through a process called reverse intersystem crossing (RISC). The small ΔE_{ST} results from the small exchange integral where the HOMO and LUMO are localized on distinct parts of the emitter molecule. The most widely employed design is based on an emitter with a strongly twisted donor–acceptor (D–A) conformation, where the HOMO will be mainly localized on the donor and the LUMO on the acceptor.

An archetype D–A TADF emitter is DMAC-TRZ, first reported by Tsai et al.³ This compound has a very small ΔE_{ST} of 0.046 eV in 8 wt % doped films in mCPCN resulting from the near orthogonal conformation between the dimethylacridine (DMAC) donor and the triazine (TRZ) acceptor. In this host, DMAC-TRZ has a sky-blue emission with a peak photoluminescence wavelength (λ_{PL}) of 495 nm and a high photoluminescence quantum yield (Φ_{PL}) of 90%. The OLEDs with this emitter showed a maximum external quantum

efficiency, EQE_{max} of 26.5% (at 1 cd m⁻²), at a λ_{EL} of 500 nm. DMAC-TRZ also exhibits very low concentration quenching, with the neat film of the material having a Φ_{PL} of 83%; the nondoped device showed an EQE_{max} of 20.0%.³ DMAC-TRZ has since been investigated extensively as the emitter in several computational and photophysical studies.^{4–6}

Many have focused on improving further the molecular design of this emitter and have investigated derivatives. Kaji and co-workers reported two modified structures of DMAC-TRZ incorporating adamantane at different positions in MA-TA,⁷ and a-DMAC-TRZ⁸ (Figure 1). In the first report, the substitution of the two distal phenyl rings on the triazine acceptor with adamantyl groups reduced the conjugation length of the acceptor, weakening it and leading to a bluer emission. Toluene solutions and neat films of MA-TA emit at 469 and 453 nm, respectively, compared to 494 and 500 nm for DMAC-TRZ. The 10 wt % doped film of MA-TA in CzSi shows a near unity Φ_{PL} of 99%, thus efficient solution-processed blue devices showed an EQE_{max} of 22.1%, at λ_{EL} of 475 nm.⁹ The functionalization of the donor in a-DMAC-TRZ

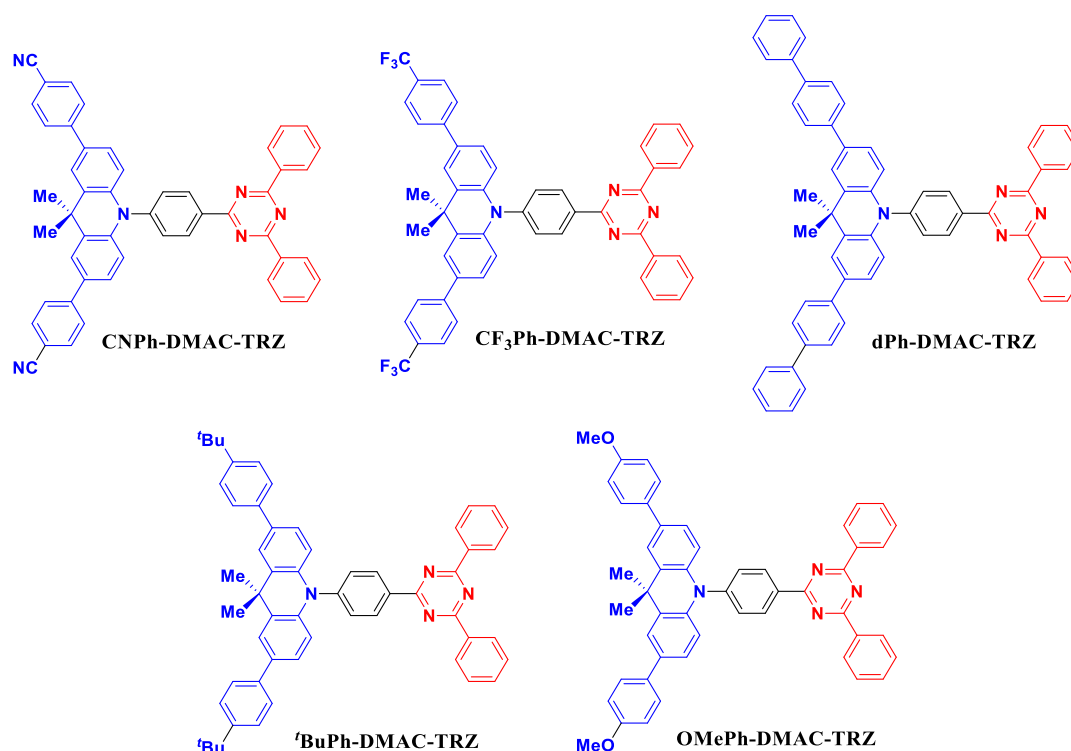


Figure 2. Chemical structures of CNPh-DMAC-TRZ, CF₃Ph-DMAC-TRZ, dPh-DMAC-TRZ, ^tBuPh-DMAC-TRZ, and OMePh-DMAC-TRZ.

increased the rigidity of the structure ultimately leading to a more efficient device than with **DMAC-TRZ**, showing an EQE_{max} of 28.9% and a λ_{EL} of 488 nm.

Kaji and co-workers reported the emitter **DMAC-bPmT**, which contains two distal pyrimidines in lieu of phenyl groups in **DMAC-TRZ**.¹⁰ The computational study revealed that the presence of these more π-accepting pyrimidines stabilizes the energy of the S₂ and T₂ states, bringing them closer in energy to the S₁ and T₁ states, which enhanced the reverse intersystem crossing rate constant (*k*_{RISC}). Indeed, experimentally *k*_{RISC} is 8.8 × 10⁵ s^{−1}, which is three times faster than the *k*_{RISC} of **DMAC-TRZ**, at 2.9 × 10⁵ s^{−1}; however, the trade-off is that the Φ_{PL} of **DMAC-bPmT** of 70% is lower (Φ_{PL} of 93% for **DMAC-TRZ**) and the emission in toluene is red-shifted at λ_{PL} of 520 nm (λ_{PL} 500 nm for **DMAC-TRZ**).

Feng et al.¹¹ described an arylmethylation strategy to enhance the horizontal orientation of the transition dipole moment (TDM) of **DMAC-TRZ** derivatives in films. **PFDMAC-TRZ** and **DPFDMAC-TRZ** (Figure 1) contain a functionalized DMAC donor containing one and two 9-phenyl-9H-fluorene groups, respectively. **PFDMAC-TRZ** and **DPFDMAC-TRZ** have the same Δ*E*_{ST} of 0.16 eV and high Φ_{PL} of 93 and 97%, respectively, in 30 wt % doped films in DPEPO. **DMAC-TRZ**, **PFDMAC-TRZ**, and **DPFDMAC-TRZ** possess anisotropy factors, *a*, of 0.29, 0.22, and 0.19, respectively, and the more horizontal orientation of the latter two was then exploited in the devices, which showed EQE_{max} values of 26.3, 35.1, and 37.0%, respectively.¹²

ToDMAC-TRZ and **PhDMAC-TRZ** are examples of two other extended **DMAC-TRZ** derivatives (Figure 1).¹³ The functionalization of **DMAC-TRZ** with either an *ortho*-tolyl unit or a phenyl unit results in a decreased Δ*E*_{ST} from 0.13 eV for **DMAC-TRZ** to 0.05 for **ToDMAC-TRZ** and 0.11 eV for **PhDMAC-TRZ**, in 30 wt % doped films in PPT. Although the Δ*E*_{ST} value of **DMAC-TRZ** here is different from the

previously reported one,³ is likely a function of a combination of the different host, emitter concentration, and measurement parameters used, in both cases, the value is very small. The λ_{PL} in these doped films is red-shifted from 510 nm for **DMAC-TRZ** to 520 and 531 nm for **ToDMAC-TRZ** and **PhDMAC-TRZ**, respectively. This is due to the strengthening of the donor due to increased conjugation between these aromatic groups and the DMAC donor core. As 30 wt % doped films in PPT, **DMAC-TRZ**, **ToDMAC-TRZ**, and **PhDMAC-TRZ** have Φ_{PL} values of 91, 99, and 73%, respectively. The trend in EQE_{max} of 18.8, 18.9, and 17.2% of the corresponding devices mirrors their Φ_{PL} while their λ_{EL} are blue-shifted at 499, 510, and 524 nm, compared to their λ_{PL}.

Here, we report a rationally designed family of **DMAC-TRZ** derivatives, **CNPh-DMAC-TRZ**, **CF₃Ph-DMAC-TRZ**, **dPh-DMAC-TRZ**, **^tBuPh-DMAC-TRZ**, and **OMePh-DMAC-TRZ** (Figure 2) wherein the central DMAC donor is decorated with two aryl groups containing at the 4-position differing electron-donating or withdrawing groups. The effect of donor decoration on the color tuning of the emitters, their triplet exciton harvesting, and PL efficiencies is demonstrated. Further, using angle-resolved photoluminescence spectroscopy, we explore how the increased molecular weight and length of the emitter (depending on the nature of the peripheral substituent on the donor) affect the orientation of its TDM. Using optical simulations, the effect of the TDM orientation on the light outcoupling efficiency is explored, revealing that its effect is minor compared to the impact of the RISC rate on the OLED efficiency.

METHODS

General Synthetic Procedures. The following starting materials were synthesized according to literature protocols, **DMAC**.¹⁴ All other reagents and solvents were obtained from commercial sources and used as received. Air-sensitive

reactions were performed under a nitrogen atmosphere using Schlenk techniques, and no special precautions were taken to exclude air or moisture during workup and crystallization. Flash column chromatography was carried out using silica gel (Silica-P from Silicycle, 60 Å, 40–63 μm). Analytical thin-layer chromatography (TLC) was performed with silica plates with aluminum backings (250 μm with F-254 indicator). TLC visualization was accomplished by a 254/365 nm UV lamp. HPLC analysis was conducted on a Shimadzu LC-40 HPLC system. HPLC traces were performed by using a Shim-pack GIST 3 μm C18 reverse-phase analytical column. GCMS analysis was conducted using a Shimadzu QP2010SE GC-MS instrument equipped with a Shimadzu SH-Rtx-1 column (30 m \times 0.25 mm). ^1H , ^{13}C , and ^{19}F NMR spectra were recorded on a Bruker Advance spectrometer (500 MHz for ^1H , 125 MHz for ^{13}C , 471 MHz for ^{19}F , and 202 MHz for ^{31}P). The following abbreviations have been used for multiplicity assignments: “s” for singlet, “d” for doublet, “t” for triplet, “q” for quartet, and “m” for multiplet. ^{19}F and ^{31}P NMR spectra were recorded with proton decoupling. ^1H and ^{13}C NMR spectra referenced residual solvent peaks with respect to TMS ($\delta = 0$ ppm). Melting points were measured using open-ended capillaries on an Electrothermal 1101D Mel-Temp apparatus and were uncorrected. High-resolution mass spectrometry (HRMS) was performed at the University of Leeds. Atmospheric pressure chemical ionization (APCI) spectra were recorded on a Bruker Impact spectrometer equipped with a direct insertion probe. Elemental analyses were performed at the School of Geosciences at the University of Edinburgh using a Thermo Fisher Scientific Flash SMART 2000 Instrument.

Electrochemistry Measurements. Cyclic voltammetry (CV) and Differential Pulse Voltammetry analyses were performed on an Electrochemical Analyzer model 620D from CH Instruments. Sample of the different materials were prepared in DCM that was degassed by sparging with DCM-saturated nitrogen gas for 10 min before measurements. All measurements were performed in 0.1 M DCM or a solution of tetrabutylammonium hexafluorophosphate, which was used as the supporting electrolyte. An Ag/Ag^+ electrode was used as the reference electrode while a glassy carbon electrode and a platinum wire were used as the working electrode and counter electrode, respectively. The redox potentials are reported relative to a saturated calomel electrode (SCE) with a ferrocene/ferrocenium (Fc/Fc^+) redox couple as the internal standard (0.46 V vs SCE for DCM).¹⁵ CV was performed with a scan rate of 100 mV/s and a sensitivity of 1×10^{-5} A/V. DPV was performed with an increment of a potential of 0.01 V, amplitude of 0.05 V, pulse width of 0.06 s, sample width of 0.02 s, pulse period 0.05 s, quiet time of 2 s, and sensitivity of 1×10^{-5} A/V.

Photophysical Measurements. Optically dilute solutions of concentrations on the order of 10^{-5} M were prepared in HPLC grade methyl-cyclohexane, toluene, DCM, THF, and MeCN for absorption and emission analysis. Absorption spectra were recorded at room temperature on a Shimadzu UV-2600 double-beam spectrophotometer with a 1 cm quartz cuvette. Molar absorptivity determination was verified by a linear least-squares fit of values obtained from at least five independent solutions at varying concentrations ranging from 1×10^{-5} to 3.34×10^{-6} M.

For emission studies, aerated solutions were bubbled with compressed air for 5 min, and spectra were taken using the

same cuvette as for the absorption analysis. Degassed solutions were prepared via three freeze–pump–thaw cycles, and spectra were taken using a homemade Schlenk quartz cuvette. Steady-state emission, excitation spectra, and time-resolved emission spectra were recorded at 298 K using an Edinburgh Instruments F980 and FSS (the latter for solvatochromism measurements). Samples were excited at 340 nm for steady-state measurements and at 378 nm for time-resolved measurements. Photoluminescence quantum yields for solutions were determined using the optically dilute method¹⁶ in which four sample solutions with absorbances of ca. 0.09, 0.07, 0.05, and 0.03 at 360 nm were used. The Beer–Lambert law was found to remain linear at the concentrations of the solutions. For each sample, linearity between absorption and emission intensity was verified through linear regression analysis with the Pearson regression factor (R^2) for the linear fit of the data set surpassing 0.9. Individual relative quantum yield values were calculated for each solution, and the values reported represent the slope obtained from the linear fit of these results. The equation $\Phi_s = \Phi_r(A_r/A_s)(I_s/I_r)(n_s/n_r)^2$ was used to calculate the relative quantum yield of the sample, where (Φ_r) is the absolute quantum yield of the external reference quinine sulfate ($\Phi_r = 54.6\%$ in 1 N H_2SO_4).¹⁷ A stands for the absorbance at the excitation wavelength, I is the integrated area under the corrected emission curve, and n is the refractive index of the solvent. The subscripts “s” and “r” represent sample and reference, respectively. The experimental uncertainty in the emission quantum yields is conservatively estimated to be 10%, though we have found that statistically, we can reproduce Φ_{PL} values to 3% relative error. Thin-film Φ_{PL} measurements were performed by using an integrating sphere in a Hamamatsu C9920-02 system. A xenon lamp coupled to a monochromator enabled excitation selectivity, chosen here to be 340 nm. The output was then fed into the integrating sphere via a fiber, exciting the sample. PL spectra were collected with a multimode fiber and detected with a back-thinned CCD. Doped thin films were prepared by mixing sample (10 wt %) and host material in Chlorobenzene solution, followed by spin-casting on a quartz substrate. The Φ_{PL} of the films were then measured in air and by purging the integrating sphere with flowing N_2 gas for 10 min. Time-resolved PL measurements of the solution samples were carried out using the time-correlated single-photon counting technique. The samples were excited at 378 nm by a pulsed laser diode (Picoquant, model PLS 370) and were kept in a vacuum of $<8 \times 10^{-4}$ mbar.

Solid-state sample time-resolved measurements were performed using a spectrograph (Horiba Triax) and a Stanford Computer Optics 4 Picos intensified charge-coupled device camera, where samples were excited with a Nd:YAG laser (EKSPLA, 10 Hz, 355 nm) under a vacuum. The singlet–triplet splitting energy, ΔE_{ST} , was estimated by recording the prompt fluorescence spectra and phosphorescence emission at 77 K.

Angular-Dependent Photoluminescence Spectroscopy. Thin films of emitter and host were co-evaporated in a high vacuum on a precleaned glass substrate. This substrate was then glued with an index-matching fluid on a fused-silica prism, which was mounted on the rotating stage. The organic film was then irradiated with a UV laser (Kimmon, HeCd laser, $\lambda = 325$ nm) under vertical incidence and was rotated from -90° to $+90^\circ$ with respect to the substrate normal. The luminescence was recorded with a grating spectrograph

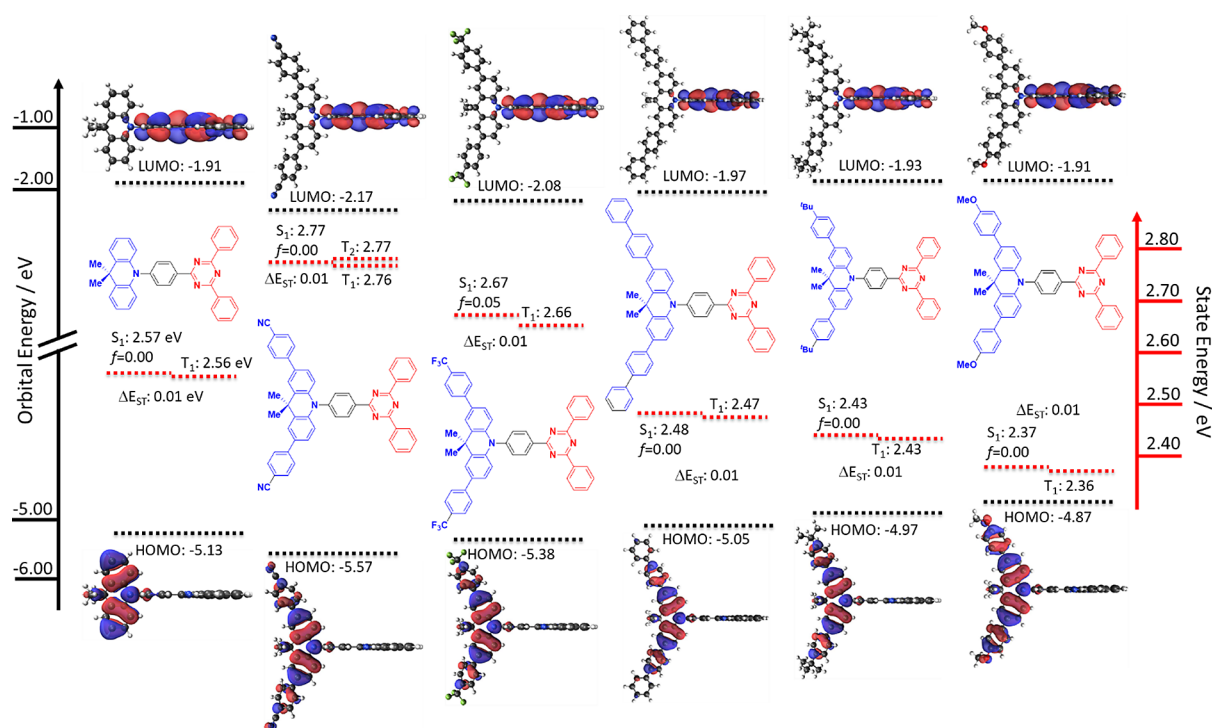


Figure 3. HOMO and LUMO electron density distributions and energy levels, excited-state energy levels of DMAC-TRZ and its five derivatives (obtained via DFT and TD-DFT at the PBE0/6-31G(d,p) level, isovalues: MO = 0.02, density = 0.0004).

coupled to a liquid-nitrogen-cooled charge-coupled device (Princeton Instruments Acton 2300i with PyLoN detector) in s- and p-polarization mode. p-polarized signal was then subjected to numerical simulation to calculate the anisotropy factor (a):

$$a = \frac{\sum p_z^2}{\sum p^2}$$

where $\sum p_z^2$ is the sum of the power emitted by vertically oriented dipoles and $\sum p^2$ is the sum of the power emitted by all emitting dipoles.¹⁸ The parameter a (or synonymously $\Theta_v = \langle \cos^2 \vartheta \rangle$) denotes the second moment of the TDM's angular distribution around the surface normal of the film, where ϑ is the angle between the molecule's TDM vector and the said direction. The details about the method can be further found in the references.^{18,19}

OLED Fabrication and Testing. OLED devices of the materials were fabricated on patterned indium tin oxide (ITO)-coated glass (VisionTek Systems) with a sheet resistance of 15 Ω /sq. After sonicating in acetone and isopropanol, oxygen-plasma-cleaned substrates were loaded into a Kurt J. Lesker Super Spectros deposition chamber, and both the small molecule and cathode layers were thermally evaporated at a pressure below 10^{-7} mbar. Devices tested in a calibrated 10 inch integrating sphere (Labsphere) and their electrical properties were measured using a source meter (Keithley 2400). Emission spectra were simultaneously measured using a calibrated fiber-coupled spectrometer (Ocean Optics USB4000). All devices were evaluated at RT (298 K) and under an air atmosphere.

Theoretical Calculations. Calculations were submitted and processed using the Silico v 0.20.5 software package^{20,21} which incorporates a number of publicly available software libraries, including: cclib²² for parsing of result files, VMD^{23/}

Tachyon²⁴ for 3D rendering, Open Babel²⁵/Pybel²⁶ for file interconversion.

All ground-state optimizations have been carried out using the density functional theory (DFT) level implemented within Gaussian 16²⁷ in the gas phase, using the PBE0²⁸ functional and the 6-31G(d,p) basis set.²⁹ Excited-state calculations were performed using TD-DFT within the Tamm–Dancoff approximation³⁰ using the same functional and basis set as for ground-state geometry optimization. This methodology has been demonstrated to show a quantitative estimate of ΔE_{ST} in comparison to the experiment.³¹

RESULTS AND DISCUSSION

Theoretical Calculations. The optoelectronic properties of DMAC-TRZ and the five new derivatives were first assessed using a combined DFT and TD-DFT theoretical study at the PBE0/6-31G(d,p)^{28,29} level (Figure 3). DMAC-TRZ has HOMO and LUMO energy levels of -5.13 and -1.91 eV, respectively. The DMAC is twisted to almost 90° with respect to the triazine, as previously observed in the literature,³ leading to a very small overlap between the HOMO located on the DMAC and the LUMO located on the triazine, and thus an almost zero ΔE_{ST} ; S_1 and T_1 levels are 2.57 and 2.56 eV, respectively. The small overlap between HOMO and LUMO also leads to an oscillator strength with a value of zero.

The ground-state optimized structures of the five derivatives all possess similar conformations as that of DMAC-TRZ, thus leading to ΔE_{ST} values of ca. 0.01 eV. As the substituents at the 4-position of the aryl groups change from electron-withdrawing (CN and CF₃) to electron-donating (^tBu and OMe) the HOMO energy level becomes progressively destabilized, with values of -5.57 , -5.38 , -5.05 , -4.97 , and -4.87 eV for CNPh-DMAC-TRZ, CF₃Ph-DMAC-TRZ, dPh-DMAC-TRZ, ^tBuPh-DMAC-TRZ, and OMePh-DMAC-TRZ, respectively.

Scheme 1. Synthetic Procedure for the Five DMAC-TRZ Derivatives

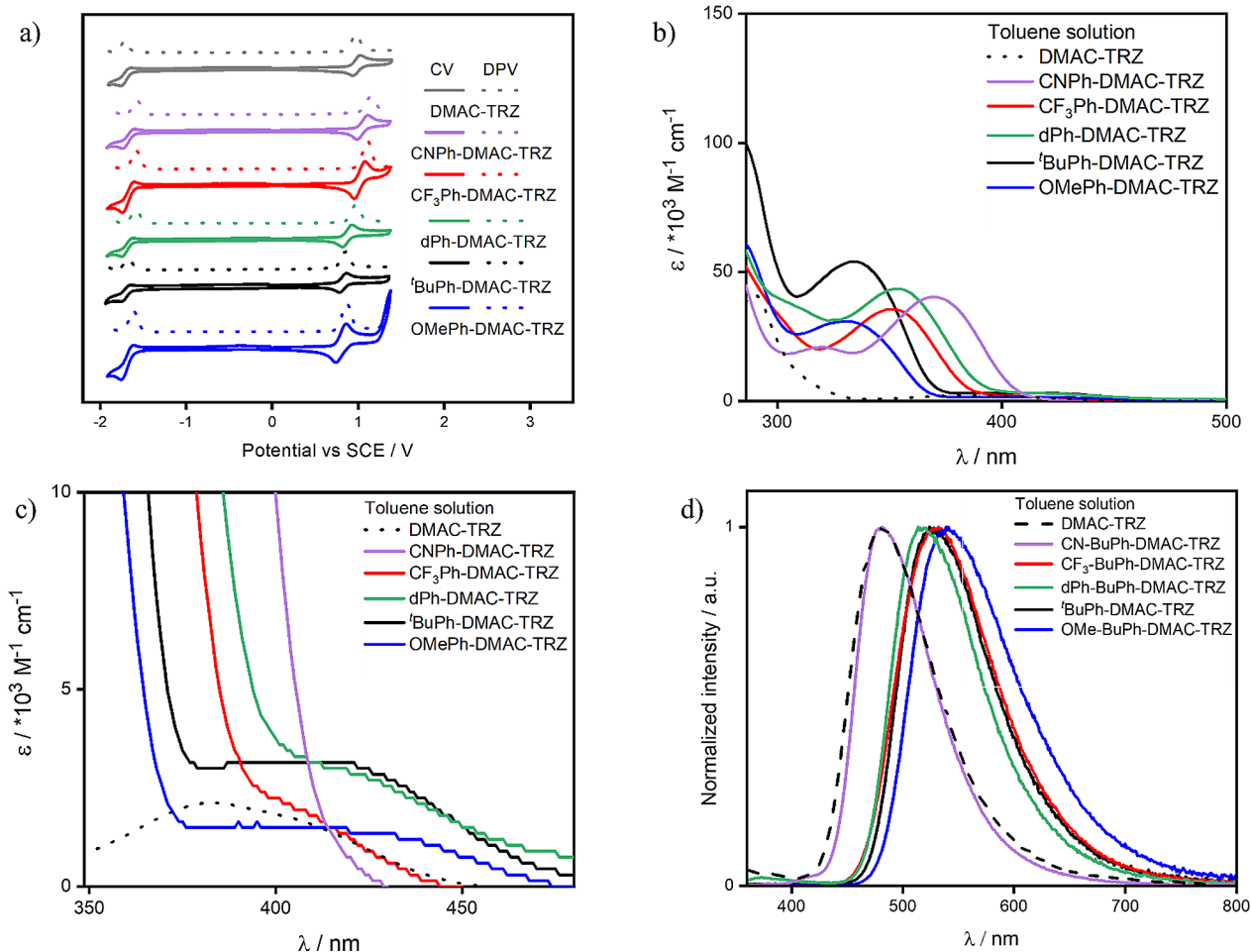
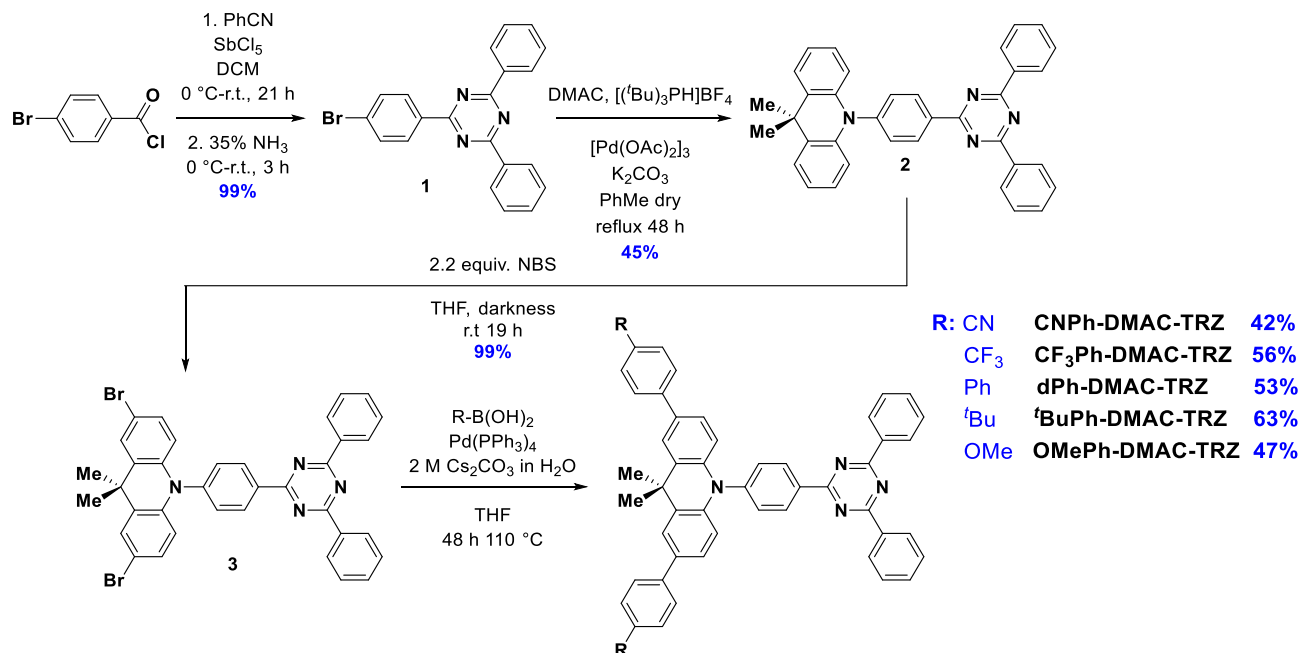


Figure 4. (a) Cyclic voltammetry (CV) and differential pulse voltammetry (DPV) of DMAC-TRZ and derivatives in DCM (scan rate = 100 mV/s); (b) UV-vis absorption spectra of DMAC-TRZ, and derivatives in toluene and (c) zoom on the low intensity CT bands; (d) photoluminescence spectra of DMAC-TRZ and its derivatives in toluene ($\lambda_{\text{exc}} = 340 \text{ nm}$, 10^{-5} M solution).

The LUMO levels are likewise destabilized along the series, although to a lesser extent than the HOMO levels as the triazine is only weakly conjugated to the DMAC-based donor. The LUMO values are -2.17 , -2.08 , -1.97 , -1.93 , and -1.91 eV for CNPh-DMAC-TRZ, CF₃Ph-DMAC-TRZ, dPh-DMAC-TRZ, ^tBuPh-DMAC-TRZ, and OMePh-DMAC-TRZ, respectively. The HOMO level of DMAC-TRZ (-5.13 eV) falls in the middle of the series between those of CF₃Ph-DMAC-TRZ and dPh-DMAC-TRZ. The LUMO of DMAC-TRZ (-1.91 eV) falls between those of dPh-DMAC-TRZ and ^tBuPh-DMAC-TRZ. The biphenyl group is an inductively electron-withdrawing moiety, which can then slightly stabilize the LUMO level, making it lower in energy than DMAC-TRZ.

The singlet and triplet energy levels are also affected by the nature of the substituent on the DMAC donor. The energies of the excited states become systematically more stable across the series (Figure 3). The S_1/T_1 energies are $2.77/2.76$, $2.67/2.66$, $2.48/2.47$, $2.37/2.36$, and $2.43/2.43$ eV for CNPh-DMAC-TRZ, CF₃Ph-DMAC-TRZ, dPh-DMAC-TRZ, ^tBuPh-DMAC-TRZ, and OMePh-DMAC-TRZ, respectively. The S_1/T_1 energies of DMAC-TRZ lie between those of CF₃Ph-DMAC-TRZ and dPh-DMAC-TRZ. All of the compounds possess S_1 and T_1 states that possess charge transfer (CT) character (HOMO \rightarrow LUMO transition). dCNPh-DMAC-TRZ is the only molecule that has a degenerate T_2 state, which has a locally excited (LE) character localized on the donor moiety (HOMO \rightarrow LUMO+2 transition). The ca. 90° conformation and very small ΔE_{ST} values of ca. 0.01 eV also lead to an effective oscillator strength value of 0.00 . The only exception is observed in CF₃Ph-DMAC-TRZ with a f of 0.05 .

Synthesis. The five DMAC-TRZ derivatives were synthesized via a four-step synthetic procedure (Scheme 1). Bromotriazine (**1**) was obtained in quantitative yield following a Lewis acid-catalyzed cyclization of 4-bromobenzoyl chloride and benzonitrile using antimony pentachloride in DCM, followed by the addition of 35% ammonia.³² Triazine is then coupled to DMAC through a Buchwald–Hartwig coupling in 45% yield.³ DMAC-TRZ (**2**) was then quantitatively dibrominated using 2.2 equiv of NBS in THF, shielded from light.³³ Finally, the DMAC-TRZ derivatives were accessed via a Suzuki–Miyaura cross-coupling of **3** with the corresponding arylboronic acid; the reaction was carried out in a pressure vessel at 110°C for 48 h to improve the yield of the coupled products. Yields for the final step ranged between c.a. 42 and 63%. The identity and purity of the compounds were confirmed by combination ^1H , ^{13}C , and ^{19}F NMR spectroscopy, Mp determination, HRMS, HPLC, and EA.

Optoelectronics Properties. CV and DPV of DMAC-TRZ (for comparison) and the five emitters (Figure 4a) were carried out in DCM. The electrochemistry of DMAC-TRZ (oxidation attributed to the DMAC and reduction attributed to the triazine) matches the previously reported data,^{3,34,35} with oxidation and reduction potentials at E_{ox} of 0.97 V and E_{red} -1.72 V, respectively (taken from DPV) versus SCE. The corresponding HOMO and LUMO energy values are -5.31 and -2.62 V.

Despite the predicted small changes in LUMO energies, there is no significant change in the reduction potentials, with values of -1.68 , -1.68 , -1.69 , -1.71 , and -1.69 V for CNPh-DMAC-TRZ, CF₃Ph-DMAC-TRZ, dPh-DMAC-TRZ, ^tBuPh-DMAC-TRZ, and OMePh-DMAC-TRZ, respectively, leading to LUMO values of around ~ -2.65 eV, comparable to that of DMAC-TRZ (-2.62 eV). The oxidation potentials

follow the trend observed for the DFT calculations, with electron-donating and conjugating groups cathodically shifting the oxidation potential, with values of 1.04 , 1.01 , 0.87 , 0.81 , and 0.79 V for CNPh-DMAC-TRZ, CF₃Ph-DMAC-TRZ, dPh-DMAC-TRZ, ^tBuPh-DMAC-TRZ, and OMePh-DMAC-TRZ, respectively. The HOMO energy levels values, obtained from these measured oxidation potentials, are -5.38 , -5.35 , -5.21 , -5.15 , and -5.13 eV for CNPh-DMAC-TRZ, CF₃Ph-DMAC-TRZ, dPh-DMAC-TRZ, ^tBuPh-DMAC-TRZ, and OMePh-DMAC-TRZ, respectively, while DMAC-TRZ falls in the middle of the series (-5.31 eV).

The UV–vis absorption of DMAC-TRZ and its five derivatives were carried out in a toluene solution (Figure 4b,c). The very low intensity of the lowest energy absorption band of DMAC-TRZ (~ 400 nm) is reflective of the orthogonal conformation between donor and acceptor. In this conformation, the poor overlap between HOMO and LUMO results in an oscillator strength of almost zero, reflected in the very low molar absorptivity for this CT transition ($\epsilon = 2000\text{ M}^{-1}\text{ cm}^{-1}$).

The absorption spectra of the five derivatives reveal the first instance of a structure–property trend that will be a staple for the series: ^tBuPh-DMAC-TRZ and OMePh-DMAC-TRZ have similar behavior, as do CF₃Ph-DMAC-TRZ, and dPh-DMAC-TRZ, while the behavior of CNPh-DMAC-TRZ is rather distinct. Distinct from the absorption spectrum of DMAC-TRZ, there is a well-defined low-energy band ($\epsilon > 10^4\text{ M}^{-1}\text{ cm}^{-1}$) in the absorption spectra of all five emitters (Figure 4b). This band is assigned to a π – π^* transition localized on the aryl-substituted DMAC donor, verified by TD-DFT calculations (Table S2).¹⁰ The donor–acceptor CT absorption bands of the five derivatives, characterized by their low energy and small extinction coefficient, are shown in Figure 4c. The CT absorption band falls around 410 nm for ^tBuPh-DMAC-TRZ, dPh-DMAC-TRZ, and OMePh-DMAC-TRZ, with ϵ values of 3050 , 3040 , and $1190\text{ M}^{-1}\text{ cm}^{-1}$, respectively. The CT band is slightly blue-shifted in CF₃Ph-DMAC-TRZ at around 400 nm ($\epsilon = 2170\text{ M}^{-1}\text{ cm}^{-1}$) and is of a similar profile to that of the highly twisted conformer of DMAC-TRZ. CNPh-DMAC-TRZ has two absorption bands, at 369 and 318 nm, assigned by TDDFT calculations (Figure S35) to different ^1LE transitions on the acridine donor to the S_3 , and S_5 states, respectively, with ϵ values of $40,150\text{ M}^{-1}\text{ cm}^{-1}$ (at 369 nm) and $20,330\text{ M}^{-1}\text{ cm}^{-1}$ (at 318 nm). The red-shifted, strong absorption bands of the CNPh-acridine donor obscure the weak ^1CT absorption.

The absorption and emission spectra of DMAC-TRZ and its five derivatives were measured in different polarity solvents (Figure S36). The absorption spectra are mostly unaffected by the solvent polarity, presumably because of the low ground-state dipole moment of these compounds, while the emission spectra follow the expected bathochromic shift with increasing solvent polarity, which is associated with excited states of CT character. Indeed, toluene, THF, and DCM solutions show broad and unstructured spectra, typical of a CT-type emission, while methyl-cyclohexane shows a narrower and more structured LE-type emission, in all cases.

The photophysics of the emitters were then investigated in a degassed toluene solution (Figure S37). DMAC-TRZ in toluene emits at 500 nm. CNPh-DMAC-TRZ, and CF₃Ph-DMAC-TRZ present blue-shifted emission (λ_{PL} of 484 and 487 nm, respectively), while the other derivatives emission is red-shifted (λ_{PL} of 511 , 518 , and 528 nm for dPh-DMAC-

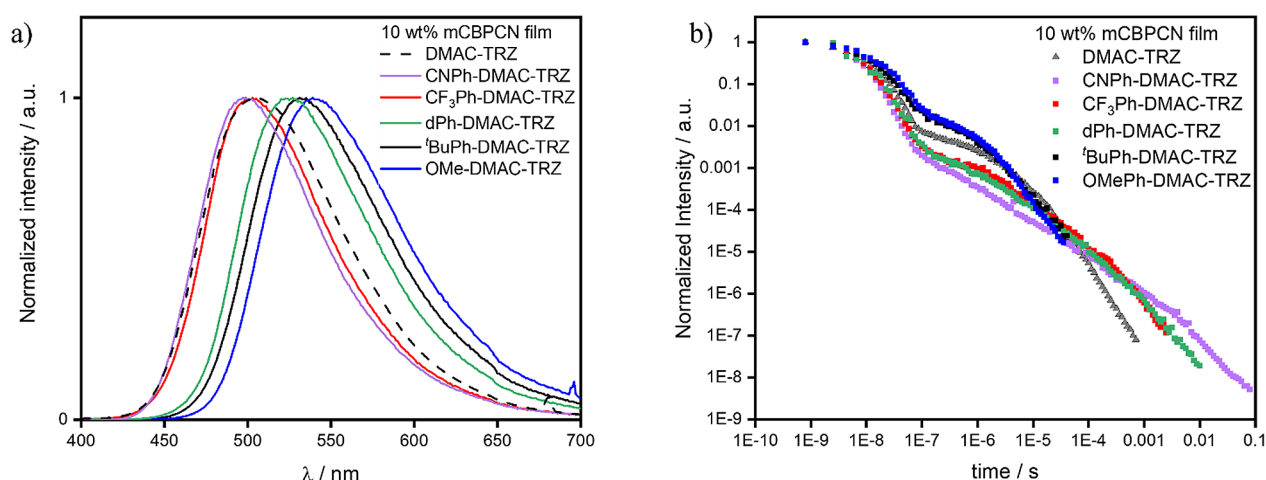


Figure 5. (a) Photoluminescence spectra and (b) time-resolved emission decays at room temperature of DMAC-TRZ and its five derivatives in 10 wt % doped films in mCBPCN ($\lambda_{\text{exc}} = 355 \text{ nm}$).

TRZ, ^tBuPh-DMAC-TRZ, and OMePh-DMAC-TRZ, respectively), compared to DMAC-TRZ (Figure 4d). DMAC-TRZ in degassed toluene solution has a Φ_{PL} of 67%, which decreases to 21% when it is exposed to air. This is lower than the literature-reported value ($\Phi_{\text{PL}} \sim 93\%$), presumably due to different excitation wavelength used and measurement methods.¹⁰ CNPh-DMAC-TRZ, CF₃Ph-DMAC-TRZ, dPh-DMAC-TRZ, ^tBuPh-DMAC-TRZ, OMePh-DMAC-TRZ have Φ_{PL} values (degassed/aerated) of 41/32, 72/28, 70/35, 74/24, and 75/23%, respectively. Thus, all compounds have larger Φ_{PL} values compared to the parent emitter, apart from CNPh-DMAC-TRZ, which also shows less sensitivity to oxygen quenching. To explore the latter, and more specifically the contribution of the delayed component, time-resolved photoluminescence measurements (TRPL) were carried out in both the degassed and aerated toluene solutions.

The TRPL of the degassed toluene solution of DMAC-TRZ possesses both prompt and delayed components with monoexponential decays and lifetimes, τ_{p} of 20.8 ns and τ_{d} of 5.21 μs , respectively (Figure S37). These lifetimes are comparable to those previously reported in the literature for the same compound.⁵ As expected, the delayed component disappears after the solution is exposed to air. The derivatives decorated with electron-donating groups have slightly longer τ_{p} than DMAC-TRZ, with monoexponential decays of 28.70 and 28.09 ns for ^tBuPh-DMAC-TRZ and OMePh-DMAC-TRZ, respectively (Figure S37). Their degassed solutions possess much shorter delayed lifetimes than DMAC-TRZ, with monoexponential τ_{d} of 2.39 and 1.49 μs , for ^tBuPh-DMAC-TRZ and OMePh-DMAC-TRZ, respectively, each of which disappears when the solution is exposed to air. This implies a more efficient reverse intersystem crossing rate (k_{RISC}) for these two emitters, as both the amplitude and the lifetime of the delayed component improve. The TRPL of CF₃Ph-DMAC-TRZ and dPh-DMAC-TRZ appears to behave in the opposite manner with shorter τ_{p} of 10.9 and 15.4 ns, respectively (Figure S37) and longer τ_{d} and biexponential decay kinetics (average τ_{d} of 20.7 and 25.8 μs , respectively), which also disappear after exposure to air. There is no delayed emission observed for CNPh-DMAC-TRZ and the τ_{p} is 8.24 ns, which decreases to 6.53 ns when exposed to air due to a small degree of singlet quenching caused by the presence of

oxygen.³⁶ The short prompt lifetime is consistent with emission from an LE state.

The photophysical properties of the materials in the solid state were first studied in the host matrix mCP (Figure S38). This host was chosen as it has a relatively high triplet energy (2.9 eV), which makes it suitable for both green and blue devices.³⁷ The Φ_{PL} of ^tBuPh-DMAC-TRZ appears to decrease slightly at concentrations above 10 wt % (Table S7). Thus, 10 wt % loading was chosen for all the emitters in mCP.⁵ The trend in the solid-state PL spectra of the six emitters at 10 wt % in mCP (Figure S38a) matches that observed in toluene (Figure 4d). Interestingly, the λ_{PL} values of DMAC-TRZ, CNPh-DMAC-TRZ, and CF₃Ph-DMAC-TRZ are almost isoenergetic in mCP (Table S6). This is attributed to the stronger intermolecular interactions taking place in the films.^{38,39}

The TRPL behavior in the mCP films is also comparable to that observed in toluene; notably, there is a small degree of delayed emission observed for CNPh-DMAC-TRZ (Figure S38). The presence of electron-donating substituents on the donor leads to a longer-lived prompt fluorescence, while the opposite trend is observed for the delayed fluorescence lifetimes. The TADF character of all of the materials was confirmed by temperature-dependent TRPL measurements, where the contribution from the delayed emission increases with increasing temperature (Figure S38). The delayed emission of both ^tBuPh-DMAC-TRZ and OMePh-DMAC-TRZ is only modestly quenched at 80 K, attributed to the highly efficient RISC process in these two emitters; thus, at this temperature, triplet harvesting is not fully suppressed.⁴⁰ This effect is also observed for their 80 K phosphorescence spectra, which are not structured, resulting in a misleading triplet energy value, while their 20 K phosphorescence spectra are more structured (indicating mixed CT/LE character) and the triplet energy value appears similar in both molecules, around 2.65 eV (Figure S39). This results in a ΔE_{ST} of 30 meV for both emitters and is in good agreement with the DFT calculations (Figure 3). For CNPh-DMAC-TRZ, CF₃Ph-DMAC-TRZ, and dPh-DMAC-TRZ, 80 K is a sufficiently low temperature to effectively suppress TADF, and structured phosphorescence is observed with energy onset at 2.5, 2.63, and 2.54 eV, respectively (Figure S39). The resulting ΔE_{ST} values are 290, 210, and 150 meV for CNPh-DMAC-TRZ,

Table 1. Kinetics Analysis³⁶ of 10 wt % Doped Films of DMAC-TRZ and Its Five Derivatives in mCBPCN

R-DMAC-TRZ	A_{PF} (a.u.)	τ_{PF} avg. ^a ($\times 10^{-9}$ s)	A_{DF} ($\times 10^{-4}$ a.u.)	τ_{DF} avg. ^a ($\times 10^{-6}$ s)	Φ_{PL} ^b (%)	Φ_{PF} ^c (%)	Φ_{DE} ^c (%)	k_F avg. ^a ($\times 10^7$ s ⁻¹)	k_{ISC} avg. ^a ($\times 10^7$ s ⁻¹)	k_{RISC} avg. ^a ($\times 10^5$ s ⁻¹)
^t BuPh-	0.88	16.2	66.1	2.64	72 \pm 5	32.6	39.4	6.19 \pm 0.3	4.69 \pm 0.5	7.59 \pm 0.5
OMePh-	0.87	18.5	92.6	1.99	72 \pm 5	34	38.1	5.41 \pm 0.2	3.99 \pm 0.4	9.59 \pm 0.6
dPh-	0.96	10.5	0.29	305	70 \pm 5	37.5	32.5	9.52 \pm 0.3	6.37 \pm 0.5	0.05 \pm 0.002
CF ₃ Ph-	0.98	9.5	0.64	163	70 \pm 5	33	37	10.5 \pm 0.6	7.71 \pm 0.6	0.12 \pm 0.01
CNPh-	0.95	7.8	0.06	1220	34 \pm 3	17	17	12.8 \pm 0.6	6.83 \pm 0.3	0.01 \pm 0.001
H-	0.89	12.1	9.87	15.6	87 \pm 5	35.8	51.2	8.30 \pm 0.4	7.08 \pm 0.3	1.49 \pm 0.1

^aAverage values were extracted from the averaging of the multiple exponentials used to fit the prompt and delayed lifetimes using the following equation:

$$\tau_{avg.} = \frac{\sum_{i=1}^n (A_i \tau_i^2)}{\sum_{i=1}^n (A_i \tau_i)}$$

^bObtained using an integrating sphere, under a nitrogen atmosphere, $\lambda_{exc} = 340$ nm. ^cObtained from the integrated prompt and delayed emission of the TRPL decays.⁴³

CF₃Ph-DMAC-TRZ, and dPh-DMAC-TRZ, respectively. From the modeled lowest triplet value of the aryl-decorated donor units (Figure S40), CNPh-DMAC, CF₃Ph-DMAC, and dPh-DMAC have more stabilized T₁ states compared to ^tBuPh-DMAC and OMePh-DMAC, these trend in a similar manner to the experimentally obtained values. Consequently, we propose that in CNPh-DMAC-TRZ, CF₃Ph-DMAC-TRZ, and dPh-DMAC-TRZ the T₁ state is localized on the aryl-decorated acridine donor, while in ^tBuPh-DMAC-TRZ and OMePh-DMAC-TRZ, the T₁ state has a mixed CT/LE character.

The Φ_{PL} values of the six emitters in 10 wt % doped films in mCP are compiled in Table S6. In all cases, the Φ_{PL} of the mCP doped films is lower than that in toluene. It has already been established that the Φ_{PL} of DMAC-TRZ is higher in higher dipole moment matrices.³ For these reasons, screening of the Φ_{PL} in high triplet energy hosts mCP, mCBPCN, and DPEO host was conducted using ^tBuPh-DMAC-TRZ as a representative example (Table S7). As well, mCBPCN and DPEO have relatively high MW and T_g , which would be beneficial to influence the horizontal orientation of the TDM of these materials.¹² At concentrations below 10 wt % the Φ_{PL} values are similar in the three hosts because the measurement error is higher.⁵ At higher concentrations, the Φ_{PL} values in mCBPCN and DPEO are similar and higher than those in mCP. Thus, mCBPCN was chosen as the host material to carry on the solid-state photophysical analysis, as DPEO is recognized to be unstable in the OLEDs and this would thus negatively impact the device lifetime.⁴¹ Furthermore, 10 wt % was chosen as the doping concentration as at this concentration there are few intermolecular interactions as already observed in films of DMAC-TRZ.^{5,42} The Φ_{PL} values in 10 wt % mCBPCN are 87, 34, 70, 70, 72, and 72% for DMAC-TRZ, CNPh-DMAC-TRZ, CF₃Ph-DMAC-TRZ, dPh-DMAC-TRZ, ^tBuPh-DMAC-TRZ, and OMePh-DMAC-TRZ, respectively (Table S6).

The 10 wt % doped films in mCBPCN of DMAC-TRZ, CNPh-DMAC-TRZ, CF₃Ph-DMAC-TRZ, dPh-DMAC-TRZ, ^tBuPh-DMAC-TRZ, and OMePh-DMAC-TRZ emit at λ_{PL} of 505, 498, 503, 527, 531, and 539 nm, respectively (Figure 5a). The emission spectra of ^tBuPh-DMAC-TRZ, OMePh-DMAC-TRZ, and dPh-DMAC-TRZ are red-shifted compared to the ones in 10 wt % mCP films, while the spectra of CF₃Ph-DMAC-TRZ and CNPh-DMAC-TRZ do not change much

(Table S6). The average room temperatures τ_{PF} are 7.8, 9.5, 10.5, 16.2, and 18.5 ns for CNPh-DMAC-TRZ, CF₃Ph-DMAC-TRZ, dPh-DMAC-TRZ, ^tBuPh-DMAC-TRZ, and OMePh-DMAC-TRZ, respectively (Table 1). As was observed in both solution and in mCP films, longer-lived prompt fluorescence is observed when the DMAC contains electron-donating substituents. The magnitude of the delayed component is similar to that of the doped mCP films for all emitters except ^tBuPh-DMAC-TRZ and OMePh-DMAC-TRZ, which have a higher DF contribution in their decay profile. The average τ_{DF} is 1.2 ms, 163, 305, 2.64, and 1.99 μ s for CNPh-DMAC-TRZ, CF₃Ph-DMAC-TRZ, dPh-DMAC-TRZ, ^tBuPh-DMAC-TRZ, and OMePh-DMAC-TRZ, respectively (Table 1). These lifetimes also follow the same trend as previously discussed for toluene, where the delayed lifetimes become shorter in emitters containing more electron-rich donors. DMAC-TRZ was measured in the same environment as a comparison, showing lifetimes that are intermediate, with average τ_{PF} and τ_{DF} of 12.1 ns and 15.6 μ s, respectively.

The decay kinetics were calculated following the method of Tsuchiya et al. (Table 1).³⁶ All materials possess k_F and a k_{ISC} of the order of 10^7 – 10^8 s⁻¹. The k_{RISC} were estimated to be 9.2×10^5 and 7.8×10^5 s⁻¹ for ^tBuPh-DMAC-TRZ and OMePh-DMAC-TRZ, respectively. These rates are four times faster compared to that of DMAC-TRZ ($k_{RISC} = 2.2 \times 10^5$ s⁻¹), and 1 order of magnitude faster than the k_{RISC} of CF₃Ph-DMAC-TRZ, dPh-DMAC-TRZ; the slowest k_{RISC} was observed for CNPh-DMAC-TRZ (Table 1). The trend in estimated k_{RISC} values aligns well with the relative magnitude of ΔE_{ST} (Figure S39).

Orientation Measurements. The orientation of the transition dipole moment (TDM) of the series of derivatives was measured in evaporated 10 wt % doped films in mCBPCN (Figure 6 and Table 2). All materials exhibit a preferential horizontal orientation of their TDM, with a values of 0.16, 0.26, 0.15, 0.25, and 0.20 for CNPh-DMAC-TRZ, CF₃Ph-DMAC-TRZ, dPh-DMAC-TRZ, ^tBuPh-DMAC-TRZ, and OMePh-DMAC-TRZ, respectively. The a value of DMAC-TRZ in the same environment of 0.21 lies in between those of the five derivatives.⁴ As previously mentioned, Tenopala-Carmona et al.¹² found that generally for emitters with MW > 600 g/mol, the anisotropy factor improves with higher MW, higher x_E/x_H (ratio of the length of the emitter to the host), and lower z_E (thickness of the emitter)¹² (Table S8). All five

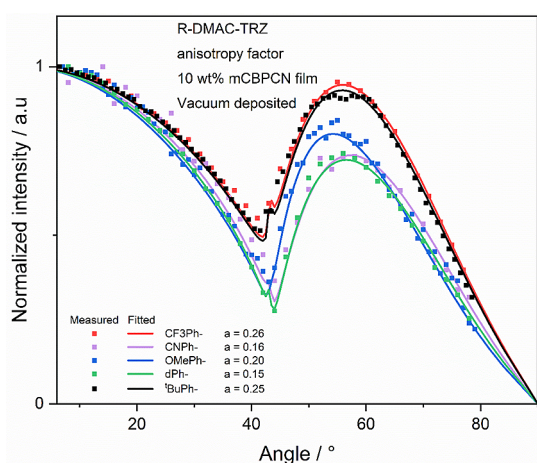


Figure 6. Angle-resolved photoluminescence measurement of CNPh-DMAC-TRZ, CF₃Ph-DMAC-TRZ, dPh-DMAC-TRZ, 'BuPh-DMAC-TRZ, and OMePh-DMAC-TRZ in evaporated 10 wt % doped films in mCBPCN. The dotted line shows the measurement, and the continuous line of the matching color shows a fit using the dipole emission model, yielding the anisotropy factor, a (data taken at λ_{PL} = 490, 500, 520, 521, and 539 nm for CNPh-DMAC-TRZ, CF₃Ph-DMAC-TRZ, dPh-DMAC-TRZ, 'BuPh-DMAC-TRZ, OMePh-DMAC-TRZ, respectively).

Table 2. Orientation Data of the Five Derivatives Obtained from Angle-Resolved Photoluminescence Measurements in Evaporated 10 wt % Doped Films in mCBPCN

emitter	a^a	θ_h^b	S^c
CNPh-DMAC-TRZ	0.16 ± 0.019	0.84	−0.275
CF ₃ Ph-DMAC-TRZ	0.26 ± 0.008	0.74	−0.11
dPh-DMAC-TRZ	0.15 ± 0.010	0.85	−0.29
'BuPh-DMAC-TRZ	0.25 ± 0.010	0.75	−0.13
OMePh-DMAC-TRZ	0.20 ± 0.022	0.80	−0.22
DMAC-TRZ	0.21 ± 0.020	0.79	−0.19

^aAnisotropy factor. ^bFraction of horizontal dipole ($\theta_h = 1 - a$).

^cOrientation order parameter ($S = (3a - 1)/2$).

derivatives (as well as the parent compound DMAC-TRZ) have the same z_E value; thus, it will not be considered in this analysis. The orthogonal conformation of the material means that the donor is responsible for the width of the material (y_E) and the thickness of the material is dependent on the triazine, which is the same in all materials. The material with the lowest a value is dPh-DMAC-TRZ, which can be rationalized as it is the heaviest material (MW of 821.02 g/mol) and has the highest x_E/x_H value of the series ($x_E/x_H = 1.35$). However, the material with the second lowest a value is CNPh-DMAC-TRZ,

which is the lightest material (MW of 718.84 g/mol) and has the smallest x_E/x_H value of the series ($x_E/x_H = 1.08$). The other materials that are categorized, in increasing a , are OMePh-DMAC-TRZ ($a = 0.19$), 'BuPh-DMAC-TRZ ($a = 0.25$), and CF₃Ph-DMAC-TRZ ($a = 0.26$); no discernible trend was identified for these materials. Furthermore, DMAC-TRZ (MW = 516.63 g/mol) is even lighter than all its derivatives but still has an appreciable orientation factor ($a = 0.21$). Thus, the simple geometrical arguments do not apply here.

OLEDs. OLEDs were fabricated with the following architecture: ITO/NPB (35 nm)/NPB:mCBP 1:1 (5 nm)/mCBP (10 nm)/mCBPCN:R-DMAC-TRZ x wt % (30 nm)/T2T (10 nm)/T2T:LiQ 1:1 (35 nm)/LiQ (1 nm)/Al (100 nm) (Figure S41). Initially, the OLEDs of 'BuPh-DMAC-TRZ at different doping concentrations were fabricated (Figure S42). While the efficiency roll-off improves at higher emitter doping concentrations, the overall efficiency significantly decreases with increasing emitter doping, from 10 wt % to the nondoped device, with an EQE_{max} of 28, 21, 18.6, 11.8, and 6.1% for the devices with 10, 20, 30, 60 wt % doping and nondoped device, respectively. From the 10 wt % to the nondoped device, a redshift of ca. 10 nm is observed. Thus, OLEDs of the five derivatives, at 10 wt % concentration, were fabricated.

The performance of the OLEDs is summarized in Table 3. All devices have similar turn-on voltage between 3.2 and 3.4 V, and the electroluminescence maxima (λ_{EL}) followed the same trend observed in the thin film SSPL (Figure 7a). The λ_{EL} was 501, 496, 498, 525, 526, and 531 nm for the DMAC-TRZ, CNPh-DMAC-TRZ, CF₃Ph-DMAC-TRZ, dPh-DMAC-TRZ, 'BuPh-DMAC-TRZ, and OMePh-DMAC-TRZ OLEDs, respectively.

The 'BuPh-DMAC-TRZ and OMePh-DMAC-TRZ devices showed the highest EQE_{max} of 28 and 27.4%, respectively, which is an improvement over the 26% for the device with DMAC-TRZ (Figure 7c). The CF₃Ph-DMAC-TRZ and dPh-DMAC-TRZ devices showed lower EQE_{max} values of 18.5 and 21.6%, respectively, while the worst-performing device was the one with CNPh-DMAC-TRZ, with an EQE_{max} value of 8.3%, which reflects the poor exciton harvesting ability of the emitter. These results are in good agreement with the photophysical properties of the six emitters. At 1000 cd m^{−2} the EQE of the six OLEDs was 20, 3.3, 12.8, 12.0, 21.5, and 22.1% for DMAC-TRZ, CNPh-DMAC-TRZ, CF₃Ph-DMAC-TRZ, dPh-DMAC-TRZ, 'BuPh-DMAC-TRZ, and OMePh-DMAC-TRZ respectively (Table 3). This verifies that at higher current densities, the device roll-off is proportional to the triplet harvesting efficiency (k_{RISC}) of each individual emitter

Table 3. Performance Metrics of the Corresponding OLEDs

emitter	λ_{EL}/nm^a	V_{on}/V	EQE _{max} /%	EQE ₁₀₀₀ /%	CE _{max} /cd A ^{−1}	PE _{max} /lm W ^{−1}	$L_{max}/cd m^{-2}$	CIE(x, y) ^a	LT ₈₅ /h ^a
DMAC-TRZ	501	3.3	26 ± 3	20 ± 1.1	67 ± 6	45.5 ± 6	21,600	0.22; 0.48	1.1
CNPh-DMAC-TRZ	496	3.4	8.3 ± 1	3.3 ± 0.3	22.5 ± 3	16 ± 3	10,000	0.20; 0.39	0.9
CF ₃ Ph-DMAC-TRZ	498	3.3	18.5 ± 1.9	12.8 ± 0.8	54.6 ± 5	40.8 ± 5	13,200	0.22; 0.48	0.2
dPh-DMAC-TRZ	525	3.2	21.6 ± 3.1	12.0 ± 1	63 ± 6	49.5 ± 6	16,200	0.29; 0.55	1.9
'BuPh-DMAC-TRZ	526	3.2	28 ± 3.3	21.5 ± 1.4	76.6 ± 6	50.1 ± 6	36,000	0.30; 0.56	0.6
OMePh-DMAC-TRZ	531	3.2	27.4 ± 3.3	22.1 ± 1.4	80.3 ± 6	54.9 ± 6	29,300	0.34; 0.57	0.3

^aRecorded at 10 mA/cm², time necessary for the emission intensity (I) to decrease to 85% of its initial value (I_0), I_0 is the luminance value taken at a current density of 10 mA/cm², which corresponds to 957, 2891, 2860, 4113, 5099, and 5743 cd m^{−2} for CNPh-DMAC-TRZ, CF₃Ph-DMAC-TRZ, dPh-DMAC-TRZ, DMAC-TRZ, 'BuPh-DMAC-TRZ, and OMePh-DMAC-TRZ.

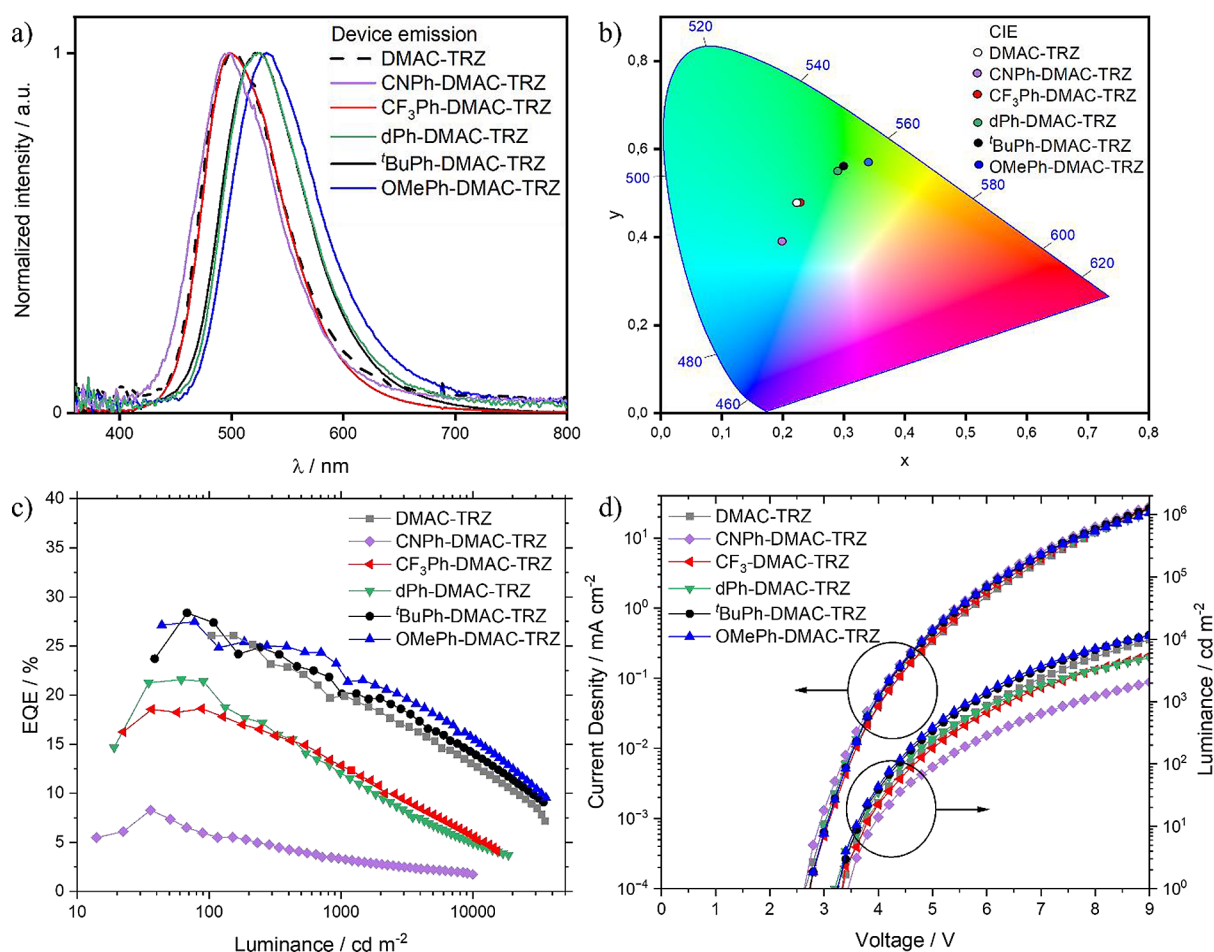


Figure 7. (a) Electroluminescence spectra (at 1000 cd m⁻²) of CNPh-DMAC-TRZ, CF₃Ph-DMAC-TRZ, dPh-DMAC-TRZ, ^tBuPh-DMAC-TRZ, OMePh-DMAC-TRZ 10 wt % doped in mCBPCN; (b) CIE coordinates of the devices (the CIE coordinates of the devices with DMAC-TRZ and CF₃Ph-DMAC-TRZ are identical, precisely under the white dot); (c) EQE vs luminance curves of the OLEDs with DMAC-TRZ and its derivatives; and (d) current density vs voltage vs luminance curves of the OLEDs.

(^tBuPh-DMAC-TRZ, OMePh-DMAC-TRZ > DMAC-TRZ > CF₃Ph-DMAC-TRZ, dPh-DMAC-TRZ > CNPh-DMAC-TRZ).

Considering the variation of the EQE_{max} values across the OLEDs with the six emitters we have performed simulations of the light outcoupling factor as a function of TDM orientation (Figure S43). The light outcoupling efficiency was estimated to be 26, 22, 28, 24, 24, and 26%, for CNPh-DMAC-TRZ, CF₃Ph-DMAC-TRZ, dPh-DMAC-TRZ, DMAC-TRZ, ^tBuPh-DMAC-TRZ, and OMePh-DMAC-TRZ, respectively (Table S9). These results predict a small improvement in the outcoupling efficiency in CNPh-DMAC-TRZ, dPh-DMAC-TRZ, and OMePh-DMAC-TRZ compared to DMAC-TRZ. However, despite their extended molecular length, the light outcoupling efficiencies of the devices with CF₃Ph-DMAC-TRZ and ^tBuPh-DMAC-TRZ are, respectively, similar, or only slightly lower than the device with DMAC-TRZ. This makes the triplet harvesting efficiency of these emitters the main parameter that determines the EQE_{max} values of the devices. It is furthermore apparent from the light outcoupling simulations that the best devices with their measured EQEs in the range of 26–28% must basically have balanced carrier recombination as well as complete triplet harvesting.

CONCLUSIONS

In this study, we report five modified DMAC-TRZ derivatives, CNPh-DMAC-TRZ, CF₃Ph-DMAC-TRZ, dPh-DMAC-TRZ, ^tBuPh-DMAC-TRZ, and OMePh-DMAC-TRZ, bearing substituted acridine donors, to explore the impact of the substitution on their photophysical and orientation properties and the impact in the performance of the OLEDs. The emission was modulated from sky blue to green in 10 wt % doped films in mCBPCN as a function of the nature of the substituent. The trend in tuning the energy of the lowest singlet excited state did not match that of tuning the energy of the lowest triplet excited state, as these states have contrasting charge-transfer and locally excited characters, respectively. This behavior results in a wide variation of the ΔE_{ST} across the five derivatives, and accordingly of k_{RISC} values (ranging from 10³ to 10⁶ s⁻¹ for CNPh-DMAC-TRZ to OMePh-DMAC-TRZ, respectively), while the Φ_{PL} values are maintained around 70% in all compounds, except CNPh-DMAC-TRZ (34%) and DMAC-TRZ (87%). Angle-resolved PL measurements of the 10 wt % emitter in mCBPCN films revealed preferentially horizontally orientated TDMs for CNPh-DMAC-TRZ, dPh-DMAC-TRZ, and OMe-DMAC-TRZ compared to DMAC-TRZ; however, this is not the case for the CF₃Ph-DMAC-TRZ and ^tBuPh-DMAC-TRZ films. This translates to a small improvement in the light outcoupling efficiency for the OLEDs

with CNPh-DMAC-TRZ, dPh-DMAC-TRZ, and OMe-DMAC-TRZ (estimated from the light outcoupling simulations), compared to the device with DMAC-TRZ; however, this was not the case for the devices with CF₃Ph-DMAC-TRZ and ^tBuPh-DMAC-TRZ.

Our study demonstrates that by decorating the donor with aryl groups in a D–A TADF emitter, the probability of achieving a higher horizontal orientation of the TDM can be improved but is highly dependent on the nature of the attached aryl group. Nevertheless, the dominant effect on OLED efficiency results from triplet harvesting whereby ^tBuPh-DMAC-TRZ and OMe-DMAC-TRZ have the fastest RISC rates and, consequently, show the highest EQE_{max} of ~28% and suppressed efficiency roll-off compared to the reference DMAC-TRZ OLEDs.

■ ASSOCIATED CONTENT

Data Availability Statement

The research data supporting this publication can be accessed at <https://doi.org/10.17630/020b200d-1928-4aea-8ebf-cb20c6cfc201>.

SI Supporting Information

The Supporting Information is available free of charge at <https://pubs.acs.org/doi/10.1021/acs.jpcc.4c03344>.

General methods; experimental section (¹H and ¹³C NMR spectra, HRMS, EA, and HPLC of all target compounds); supplementary computational data; supplementary photophysical data; supplementary OLED data; outcoupling efficiency estimation; supplementary OLED lifetime data (PDF)

XYZ combined data (TXT)

■ AUTHOR INFORMATION

Corresponding Authors

Kleitos Stavrou – OEM group, Department of Physics, Durham University, Durham DH1 3LE, U.K.; orcid.org/0000-0001-5868-3324; Email: kleitos.stavrou@durham.ac.uk

Wolfgang Brütting – Experimental Physics IV, Institute of Physics, University of Augsburg, Augsburg 86159, Germany; orcid.org/0000-0001-9895-8281; Email: wolfgang.bruetting@physik.uni-augsburg.de

Andrew Monkman – OEM group, Department of Physics, Durham University, Durham DH1 3LE, U.K.; orcid.org/0000-0002-0784-8640; Email: a.p.monkman@durham.ac.uk

Eli Zysman-Colman – Organic Semiconductor Centre, EaStCHEM School of Chemistry, University of St Andrews, St Andrews, Fife KY16 9ST, U.K.; orcid.org/0000-0001-7183-6022; Phone: +44 (0)1334 463826; Email: eli.zysman-colman@st-andrews.ac.uk

Authors

Ettore Crovini – Organic Semiconductor Centre, EaStCHEM School of Chemistry, University of St Andrews, St Andrews, Fife KY16 9ST, U.K.

Prakhar Sahay – Experimental Physics IV, Institute of Physics, University of Augsburg, Augsburg 86159, Germany

Binh Minh Nguyen – Experimental Physics IV, Institute of Physics, University of Augsburg, Augsburg 86159, Germany

Thomas Comerford – Organic Semiconductor Centre, EaStCHEM School of Chemistry, University of St Andrews, St Andrews, Fife KY16 9ST, U.K.

Stuart Warriner – School of Chemistry, University of Leeds, Leeds LS2 9JT, U.K.

Complete contact information is available at:

<https://pubs.acs.org/10.1021/acs.jpcc.4c03344>

Notes

The authors declare no competing financial interest.

■ ACKNOWLEDGMENTS

This project has received funding from the European Union's Horizon 2020 research and innovation programme under the Marie Skłodowska Curie grant agreement no. 812872 (TADFlife). A.P.M. acknowledges the Engineering and Physical Sciences Research Council for funding through the grant EP/T02240X/1. E.Z.-C. acknowledges the Engineering and Physical Sciences Research Council for support through grants EP/P010482/1 and EP/W007517/1. W.B. acknowledges funding by Deutsche Forschungsgemeinschaft (DFG) under grant numbers 341263954 and 449697195.

■ REFERENCES

- (1) Wong, M. Y.; Zysman-Colman, E. Purely Organic Thermally Activated Delayed Fluorescence Materials for Organic Light-Emitting Diodes. *Adv. Mater.* **2017**, 29, No. 1605444.
- (2) Salehi, A.; Fu, X.; Shin, D. H.; So, F. Recent Advances in OLED Optical Design. *Adv. Funct. Mater.* **2019**, 29 (15), 1–21.
- (3) Tsai, W. L.; Huang, M. H.; Lee, W. K.; Hsu, Y. J.; Pan, K. C.; Huang, Y. H.; Ting, H. C.; Sarma, M.; Ho, Y. Y.; Hu, H. C.; Chen, C. C.; Lee, M. T.; Wong, K. T.; Wu, C. C. A Versatile Thermally Activated Delayed Fluorescence Emitter for Both Highly Efficient Doped and Non-Doped Organic Light Emitting Devices. *Chem. Commun.* **2015**, 51 (71), 13662–13665.
- (4) Naqvi, B. A.; Schmid, M.; Crovini, E.; Sahay, P.; Naujoks, T.; Rodella, F.; Zhang, Z.; Strohrriegel, P.; Bräse, S.; Zysman-Colman, E.; Brütting, W. What Controls the Orientation of TADF Emitters? *Front. Chem.* **2020**, 8, 750.
- (5) Stavrou, K.; Franca, L. G.; Monkman, A. P. Photophysics of TADF Guest-Host Systems: Introducing the Idea of Hosting Potential. *ACS Appl. Electron. Mater.* **2020**, 2 (9), 2868–2881.
- (6) Dhali, R.; Phan Huu, D. K. A.; Bertocchi, F.; Sissa, C.; Terenziani, F.; Painelli, A. Understanding TADF: A Joint Experimental and Theoretical Study of DMAC-TRZ. *Phys. Chem. Chem. Phys.* **2021**, 23 (1), 378–387.
- (7) Wada, Y.; Kubo, S.; Kaji, H. Adamantyl Substitution Strategy for Realizing Solution-Processable Thermally Stable Deep-Blue Thermally Activated Delayed Fluorescence Materials. *Adv. Mater.* **2018**, 30 (8), No. 1705641.
- (8) Li, W.; Cai, X.; Li, B.; Gan, L.; He, Y.; Liu, K.; Chen, D.; Wu, Y. C.; Su, S. J. Adamantane-Substituted Acridine Donor for Blue Dual Fluorescence and Efficient Organic Light-Emitting Diodes. *Angew. Chemie - Int. Ed.* **2019**, 58 (2), 582–586.
- (9) Chen, W. C.; Lee, C. S.; Tong, Q. X. Blue-Emitting Organic Electrofluorescence Materials: Progress and Prospective. *J. Mater. Chem. C* **2015**, 3 (42), 10957–10963.
- (10) Wada, Y.; Nakagawa, H.; Kaji, H. Acceleration of Reverse Intersystem Crossing Using Different Types of Charge Transfer States. *Chem. - An Asian J.* **2021**, 16 (9), 1073–1076.
- (11) Feng, Q.; Qian, Y.; Wang, H.; Hou, W.; Peng, X.; Xie, S.; Wang, S.; Xie, L. Donor Arylmethylation toward Horizontally Oriented TADF Emitters for Efficient Electroluminescence with 37% External Quantum Efficiency. *Adv. Opt. Mater.* **2022**, 10 (10), 1–9.
- (12) Tenopala-Carmona, F.; Lee, O. S.; Crovini, E.; Neferu, A. M.; Murawski, C.; Olivier, Y.; Zysman-Colman, E.; Gather, M. C.

Identification of the Key Parameters for Horizontal Transition Dipole Orientation in Fluorescent and TADF Organic Light-Emitting Diodes. *Adv. Mater.* **2021**, *33* (37), No. 2100677.

(13) Liu, T.; Deng, C.; Duan, K.; Tsuboi, T.; Niu, S.; Wang, D.; Zhang, Q. Zero-Zero Energy-Dominated Degradation in Blue Organic Light-Emitting Diodes Employing Thermally Activated Delayed Fluorescence. *ACS Appl. Mater. Interfaces* **2022**, *14* (19), 22332–22340.

(14) Takahashi, T.; Shizu, K.; Yasuda, T.; Togashi, K.; Adachi, C. Donor–Acceptor-Structured 1,4-Diazatriphenylene Derivatives Exhibiting Thermally Activated Delayed Fluorescence: Design and Synthesis, Photophysical Properties and OLED Characteristics. *Sci. Technol. Adv. Mater.* **2014**, *15* (3), No. 034202.

(15) Connelly, N. G.; Geiger, W. E. Chemical Redox Agents for Organometallic Chemistry. *Chem. Rev.* **1996**, *96* (2), 877–910.

(16) Crosby, G. A.; Demas, J. N. Measurement of Photoluminescence Quantum Yields. *Review. J. Phys. Chem.* **1971**, *75* (8), 991–1024.

(17) Melhuish, W. H. Quantum Efficiencies of Fluorescence of Organic Substances: Effect of Solvent and Concentration of the Fluorescent Solute. *J. Phys. Chem.* **1961**, *65* (2), 229–235.

(18) Frischeisen, J.; Yokoyama, D.; Adachi, C.; Brütting, W. Determination of Molecular Dipole Orientation in Doped Fluorescent Organic Thin Films by Photoluminescence Measurements. *Appl. Phys. Lett.* **2010**, *96* (7), No. 073302.

(19) Schmidt, T. D.; Lampe, T.; M. R., D. S.; Djurovich, P. I.; Thompson, M. E.; Brütting, W. Emitter Orientation as a Key Parameter in Organic Light-Emitting Diodes. *Phys. Rev. Appl.* **2017**, *8* (3), 37001.

(20) Zysman-Colman, O. S. L. *E. Silico (Version 4)*; DigichemCo: St Andrews, 2023.

(21) Lee, O. S.; Gather, M.; Zysman-Colman, E. *Digital Discovery*, **2024**, DOI: 10.1039/D4DD00147H.

(22) O'Boyle, N. M.; Tenderholt, A. L.; Langner, K. M. Cclib A Library for Package-independent Computational Chemistry Algorithms. *Pdf. Journal of Computational Chemistry*. **2008**, *29*, 839–845.

(23) Humphrey, W.; Dalke, A.; Schulten, K. VMD: Visual Molecular Dynamics. *J. Mol. Graph.* **1996**, *14* (1), 33–38.

(24) Stone, J. TACHYON: An Efficient Library for Parallel Ray Tracing and Animation. Master's thesis, Computer Science Department, University of Missouri-Rolla, 1998.

(25) O'Boyle, N. M.; Banck, M.; James, C. A.; Morley, C.; Vandermeersch, T.; Hutchison, G. R. Open Babel: An open chemical toolbox. *J. Cheminform.* **2011**, *3*, 33.

(26) O'Boyle, N. M.; Hutchison, G. R. Cinfony - Combining Open Source Cheminformatics Toolkits behind a Common Interface. *Chem. Cent. J.* **2008**, *2* (1), 1–10.

(27) Frisch, M. J.; Trucks, G. W.; Schlegel, H. B.; Scuseria, G. E.; Robb, M. A.; Cheeseman, J. R.; Scalmani, G.; Barone, V.; Petersson, G. A.; Nakatsuji, H.; Li, X.; Caricato, M.; Marenich, A. V.; Bloino, J.; Janesko, B. G.; Gomperts, R.; Mennucci, B.; Hratchian, H. P.; Ortiz, J. V.; Izmaylov, A. F.; Sonnenberg, J. L.; Williams, Ding, F.; Lipparini, F.; Egidi, F.; Goings, J.; Peng, B.; Petrone, A.; Henderson, T.; Ranasinghe, D.; Zakrzewski, V. G.; Gao, J.; Rega, N.; Zheng, G.; Liang, W.; Hada, M.; Ehara, M.; Toyota, K.; Fukuda, R.; Hasegawa, J.; Ishida, M.; Nakajima, T.; Honda, Y.; Kitao, O.; Nakai, H.; Vreven, T.; Throssell, K.; Montgomery, Jr., J. A.; Peralta, J. E.; Ogliaro, F.; Bearpark, M. J.; Heyd, J. J.; Brothers, E. N.; Kudin, K. N.; Staroverov, V. N.; Keith, T. A.; Kobayashi, R.; Normand, J.; Raghavachari, K.; Rendell, A. P.; Burant, J. C.; Iyengar, S. S.; Tomasi, J.; Cossi, M.; Millam, J. M.; Klene, M.; Adamo, C.; Cammi, R.; Ochterski, J. W.; Martin, R. L.; Morokuma, K.; Farkas, O.; Foresman, J. B.; Fox, D. J. *G16_C01. p Gaussian 16, Revision C.01*; Gaussian, Inc.: Walling, 2016.

(28) Adamo, C.; Barone, V. Toward Reliable Density Functional Methods without Adjustable Parameters: The PBE0Model. *J. Chem. Phys.* **1999**, *110* (13), 6158–6170.

(29) Dunning, T. H. Gaussian Basis Sets for Use in Correlated Molecular Calculations. I. The Atoms Boron through Neon and Hydrogen. *J. Chem. Phys.* **1989**, *90* (2), 1007–1023.

(30) Hirata, S.; Head-Gordon, M. Time-Dependent Density Functional Theory within the Tamm-Dancoff Approximation. *Chem. Phys. Lett.* **1999**, *314* (3–4), 291–299.

(31) Moral, M.; Muccioli, L.; Son, W. J.; Olivier, Y.; Sancho-Garcia, J. C. Theoretical Rationalization of the Singlet-Triplet Gap in OLEDs Materials: Impact of Charge-Transfer Character. *J. Chem. Theory Comput.* **2015**, *11* (1), 168–177.

(32) Furue, R.; Nishimoto, T.; Park, I. S.; Lee, J.; Yasuda, T. Aggregation-Induced Delayed Fluorescence Based on Donor/Acceptor-Tethered Janus Carborane Triads: Unique Photophysical Properties of Nondoped OLEDs. *Angew. Chemie - Int. Ed.* **2016**, *55* (25), 7171–7175.

(33) Hsieh, Y. Y.; Sánchez, R. S.; Raffy, G.; Shyue, J. J.; Hirsch, L.; Del Guerso, A.; Wong, K. T.; Bassani, D. M. Supramolecular Gating of TADF Process in Self-Assembled Nano-Spheres for High-Resolution OLED Applications. *Chem. Commun.* **2022**, *58* (8), 1163–1166.

(34) Zhang, Z.; Crovini, E.; dos Santos, P. L.; Naqvi, B. A.; Cordes, D. B.; Slawin, A. M. Z.; Sahay, P.; Brütting, W.; Samuel, I. D. W.; Bräse, S.; Zysman-Colman, E. Efficient Sky-Blue Organic Light-Emitting Diodes Using a Highly Horizontally Oriented Thermally Activated Delayed Fluorescence Emitter. *Adv. Opt. Mater.* **2020**, *8* (23), No. 2001354.

(35) Hundemer, F.; Crovini, E.; Wada, Y.; Kaji, H.; Bräse, S.; Zysman-Colman, E. Tris(Triazolo)Triazine-Based Emitters for Solution-Processed Blue Thermally Activated Delayed Fluorescence Organic Light-Emitting Diodes. *Mater. Adv.* **2020**, *1* (8), 2862–2871.

(36) Tsuchiya, Y.; Diesing, S.; Bencheikh, F.; Wada, Y.; dos Santos, P. L.; Kaji, H.; Zysman-Colman, E.; Samuel, I. D. W.; Adachi, C. Exact Solution of Kinetic Analysis for Thermally Activated Delayed Fluorescence Materials. *J. Phys. Chem. A* **2021**, *125* (36), 8074–8089.

(37) Mei, L.; Hu, J.; Cao, X.; Wang, F.; Zheng, C.; Tao, Y.; Zhang, X.; Huang, W. The Inductive-Effect of Electron Withdrawing Trifluoromethyl for Thermally Activated Delayed Fluorescence: Tunable Emission from Tetra- to Penta-Carbazole in Solution Processed Blue OLEDs. *Chem. Commun.* **2015**, *51* (65), 13024–13027.

(38) Yang, J.; Fang, M.; Li, Z. Organic Luminescent Materials: The Concentration on Aggregates from Aggregation-Induced Emission. *Aggregate* **2020**, *1* (1), 6–18.

(39) Bardi, B.; Giavazzi, D.; Ferrari, E.; Iagatti, A.; Di Donato, M.; Phan Huu, D. K. A.; Di Maiolo, F.; Sissa, C.; Masino, M.; Lapini, A.; Painelli, A. Solid State Solvation: A Fresh View. *Mater. Horizons* **2023**, *10* (10), 4172–4182.

(40) Sun, D.; Duda, E.; Fan, X.; Saxena, R.; Zhang, M.; Bagnich, S.; Zhang, X.; Köhler, A.; Zysman-Colman, E. Thermally Activated Delayed Fluorescent Dendrimers That Underpin High-Efficiency Host-Free Solution-Processed Organic Light-Emitting Diodes. *Adv. Mater.* **2022**, *34*, No. 2110344.

(41) Chatterjee, T.; Wong, K. T. Perspective on Host Materials for Thermally Activated Delayed Fluorescence Organic Light Emitting Diodes. *Adv. Opt. Mater.* **2019**, *7* (1), 1–34.

(42) Stavrou, K.; Franca, L. G.; Böhmer, T.; Duben, L. M.; Marian, C. M.; Monkman, A. P. Unexpected Quasi-Axial Conformer in Thermally Activated Delayed Fluorescence DMAC-TRZ, Pushing Green OLEDs to Blue. *Adv. Funct. Mater.* **2023**, *33* (25), No. 2300910.

(43) Dias, F. B.; Penfold, T. J.; Monkman, A. P. Photophysics of Thermally Activated Delayed Fluorescence Molecules. *Methods Appl. Fluoresc.* **2017**, *5* (1), No. 012001.